Science Signaling
AAAS

www.sciencesignaling.org/cgi/content/full/11/535/eaao3134/DC1

Supplementary Materials for

Oligomerization of MrgC11 and μ-opioid receptors in sensory neurons enhances morphine analgesia

Shao-Qiu He, Qian Xu, Vinod Tiwari, Fei Yang, Michael Anderson, Zhiyong Chen, Shaness A. Grenald, Srinivasa N. Raja, Xinzhong Dong*, Yun Guan*

*Corresponding author. Email: yguan1@jhmi.edu (Y.G.); xdong2@jhmi.edu (X.D.)

Published 19 June 2018, *Sci. Signal.* **11**, eaao3134 (2018)
DOI: 10.1126/scisignal.aao3134

This PDF file includes:

Fig. S1. Colocalization of MrgC11 and MOR immunoreactivity in the mouse spinal cord.
Fig. S2. Specificity of the MOR antibody.
Fig. S3. PLA of MrgC11 and MOR in HEK293T cells.
Fig. S4. The CTD of MrgC11 mediates its interaction with MOR.
Fig. S5. Interaction of human MrgX1 and MOR.
Fig. S6. Activation of MrgC11 leads to co-internalization of MOR in DRG neurons.
Fig. S7. Internalized MrgC11 and MOR are sorted into the recycling pathway and reinserted at the cell surface.
Fig. S8. Intrathecal administration of BAM8-22 potentiates the inhibition of thermal nociception induced by low-dose morphine.
Fig. S9. Low-dose BAM8-22 alone induces minimal $[Ca^{2+}]_i$ response in DRG neurons.
Fig. S10. MrgC agonism potentiates morphine analgesia.
Fig. S11. Intrathecal coadministration of morphine and BAM8-22 does not affect exploration activity.
Fig. S12. Expression of MOR in the DRG and spinal cord of wild-type and *Mrg* KO mice.
Table S1. Behavior data associated with Fig. 6.
Table S2. Primers and oligonucleotides used for plasmid construction.
Table S3. PCR primers.

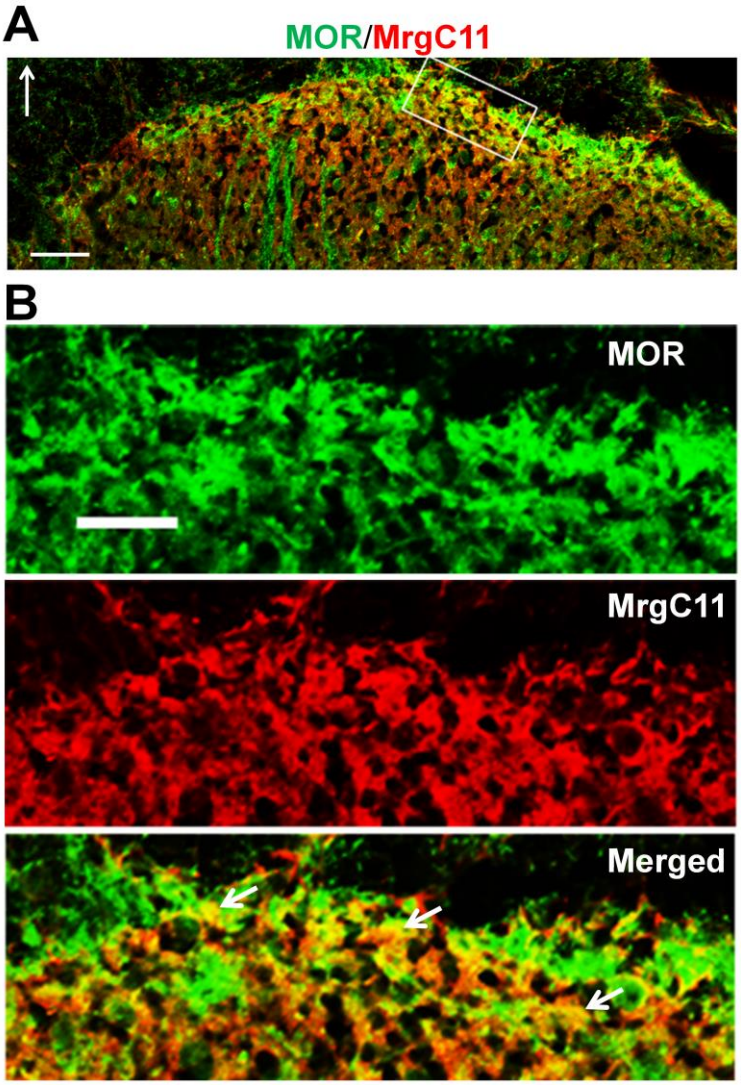

Figure S1. Colocalization of MrgC11 and MOR immunoreactivity in the mouse spinal cord. (A) Confocal image of a double immunofluorescence–stained spinal cord slice detecting MrgC11 (red) and MOR immunoreactivity (green) in superficial dorsal horn. Arrow direction indicates the dorsal side. Scale bar: 50 μm. **(B)** Higher power view of MrgC11 and MOR immunoreactivity of the boxed region in (A). Arrows: possible colocalization (yellow) of MrgC11 and MOR immunoreactivity. Scale bar: 20 μm. Data are representative of 3 experiments.

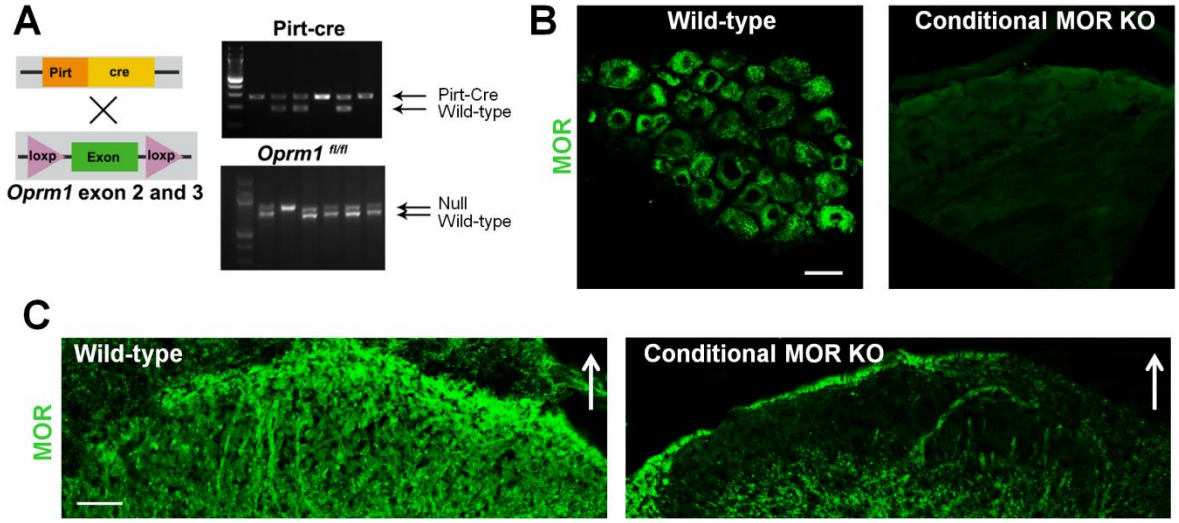

Figure S2. Specificity of the MOR antibody. (A) Left: Diagram showing the mating strategy for generating conditional MOR knockout (KO) mice: Pirt-Cre mice and *Oprm1*$^{fl/fl}$ mice were intercrossed to exclusively delete MOR expression in primary sensory neurons. Right: Genotyping of the Pirt-Cre/*Oprm1*$^{fl/fl}$ mice and wild-type mice. **(B)** Confocal images of immunofluorescence-stained DRG sections show that a subset of neurons was stained with MOR antibody in wild-type mice, but not in Pirt-Cre/*Oprm1*$^{fl/fl}$ mice. Scale bar: 40 μm. **(C)** Confocal images of MOR immunoreactivity in superficial dorsal horn of the spinal cord. Arrow direction indicates the dorsal side. Scale bar: 50 μm. Data are representative of 3 experiments.

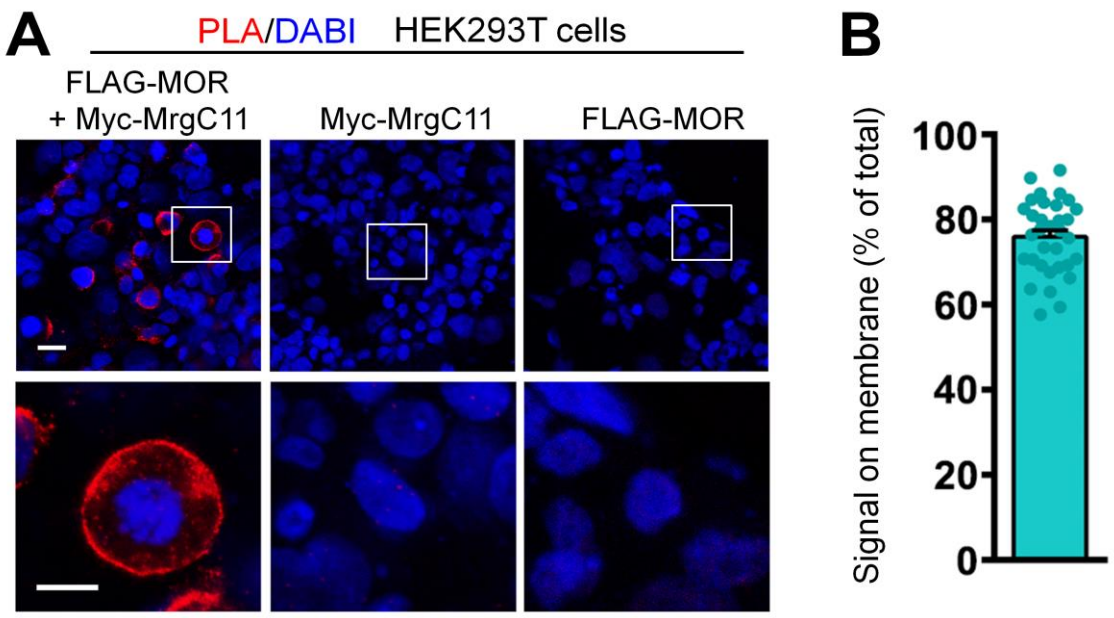

Figure S3. PLA of MrgC11 and MOR in HEK293T cells. (A) Upper: PLA signal was present only in HEK293T cells that were co-transfected with FLAG-MOR and Myc-MrgC11. Scale bar: 20 μm. Lower: A higher-power image of the boxed region. Scale bar: 10 μm. **(B)** Quantification shows that approximately 80% of the PLA signal was present near the cell membrane (n = 33). Data are mean ± SEM.

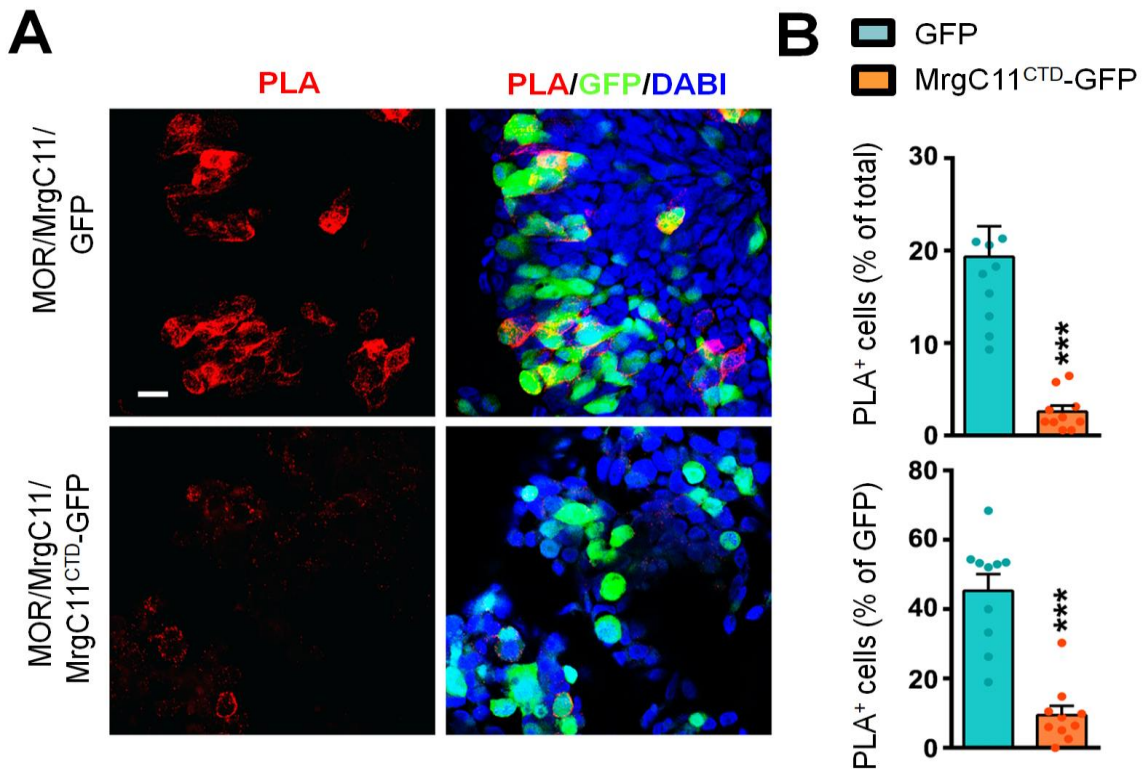

Figure S4. The CTD of MrgC11 mediates its interaction with MOR. (A) Proximity ligation assay (PLA) performed in HEK293T cells co-transfected with FLAG-MOR, Myc-MrgC11, and N1-EGFP or with FLAG-MOR, Myc-MrgC11, and MrgC11^{CTD}-GFP. The effects of expression of MrgC11 CTD on PLA signal (red) in these cells. Scale bar: 20 μm. **(B)** Quantification of the percentage of PLA-positive cells among all cells and GFP-expressing cells in the MrgC11^{CTD}-GFP and control GFP groups (n = 10 for both groups). Data are mean ± SEM. ****P* < 0.001, Student's *t* test.

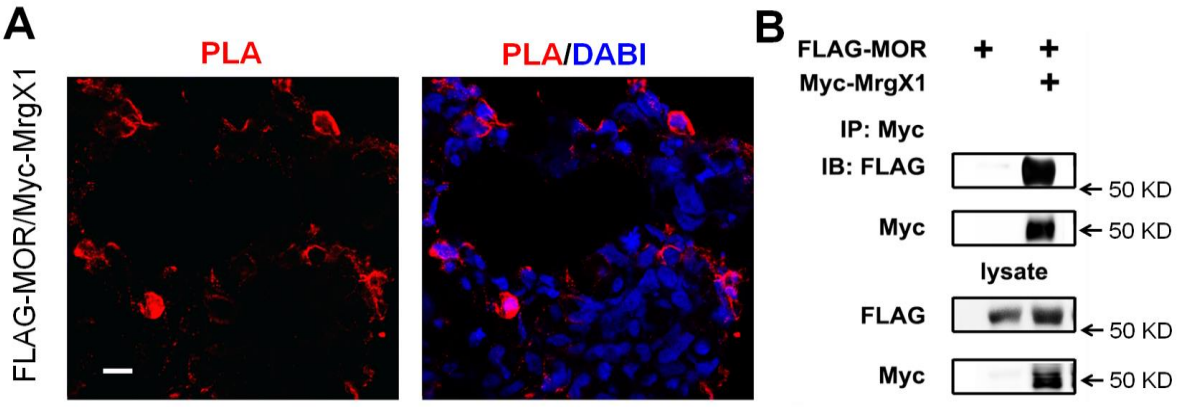

Figure S5. Interaction of human MrgX1 and MOR. (A) Proximity ligation assay (PLA) of HEK293T cells that were co-transfected with FLAG-MOR and Myc-MrgX1. Scale bar: 20 µm. **(B)** Co-Immunoprecipitation shows that Myc-MrgX1 interacts with FLAG-MOR in co-transfected HEK293T cells. IP, immunoprecipitation; IB, immunoblot. Data are representative of 3 experiments.

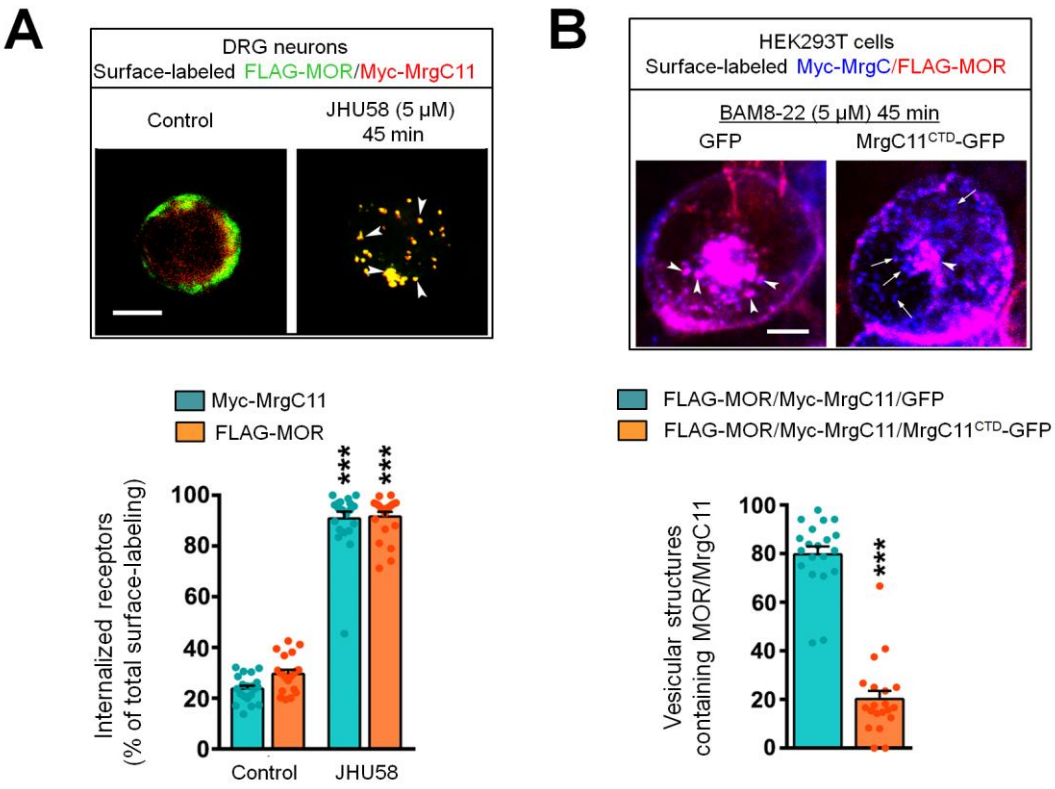

Figure S6. Activation of MrgC11 leads to co-internalization of MOR in DRG neurons. (A) Upper: In Myc-MrgC11 and FLAG-MOR co-transfected mouse DRG neurons, the receptors present on the cell surface were labeled with antibodies against FLAG (green) or Myc (red). After treatment with an MrgC agonist (JHU58, 5 μM), the prelabeled MrgC11 and MOR were co-internalized and colocalized in vesicular structures (arrowheads). Scale bar: 20 μm. Lower: Quantitative data analysis (n = 20 for control, n = 21 for JHU58). **(B)** Upper: In triple-transfected HEK293T cells, effects of co-expression of MrgC11^{CTD}-GFP and control GFP on on BAM8-22–induced co-internalization of FLAG-MOR and Myc-MrgC11. Scale bar: 10 μm. Lower: Quantitative data analysis in GFP-positive cells (n = 20 for both groups). Values are shown as mean ± SEM. ***P < 0.001, Student's t-test.

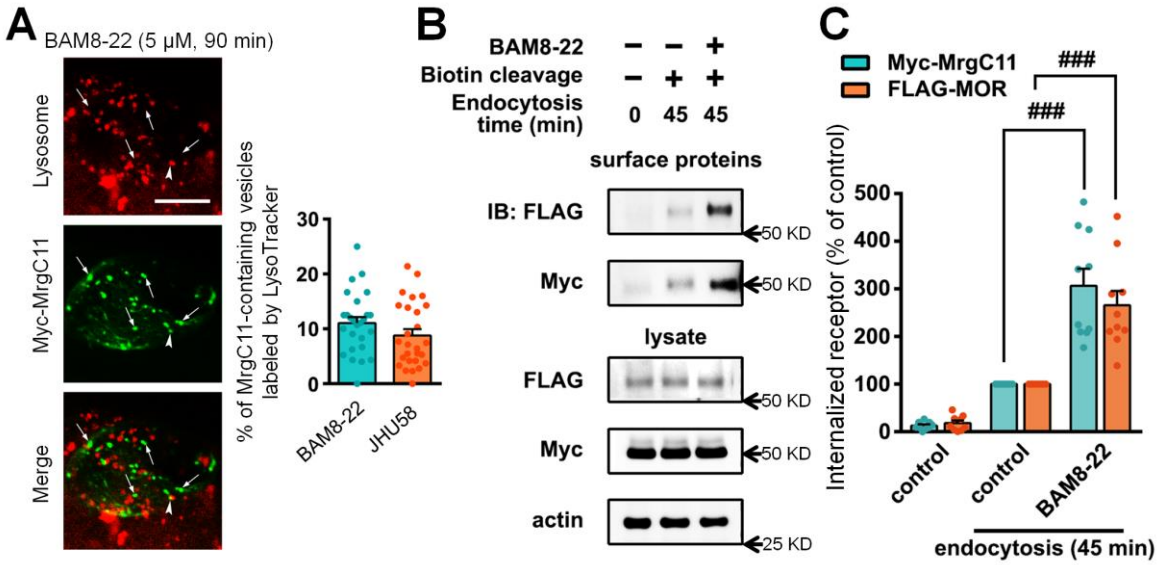

Figure S7. Internalized MrgC11 and MOR are sorted into the recycling pathway and reinserted at the cell surface. (A) Internalization of MrgC11 (arrows) in Myc-MrgC11–transfected HEK293T cells after BAM8-22 (5 μM, 90 min) and JHU58 (5 μM, 90 min) treatment. Most internalized MrgC11 was not sorted into lysosome-like compartments labeled by LysoTracker (arrowhead) (n=26). Scale bar: 10 μm. Values are mean ± SEM. **(B)** Immunoblotting (IB) showed changes in biotinylated receptors after drug treatment and biotin cleavage, which provides a measure of receptor internalization. BAM8-22 (5 μM) induced co-internalization of MrgC11 and MOR. Data are representative of 3 experiments. **(C)** Quantitative analysis of receptor recycling showed that the percentages of internalized MrgC11 and MOR after 45 min of stimulation with BAM8-22 (5 μM) or control (n = 11-13/group). Values are shown as mean ± SEM. $^{###}P < 0.001$, one-way ANOVA and Bonferroni post hoc test.

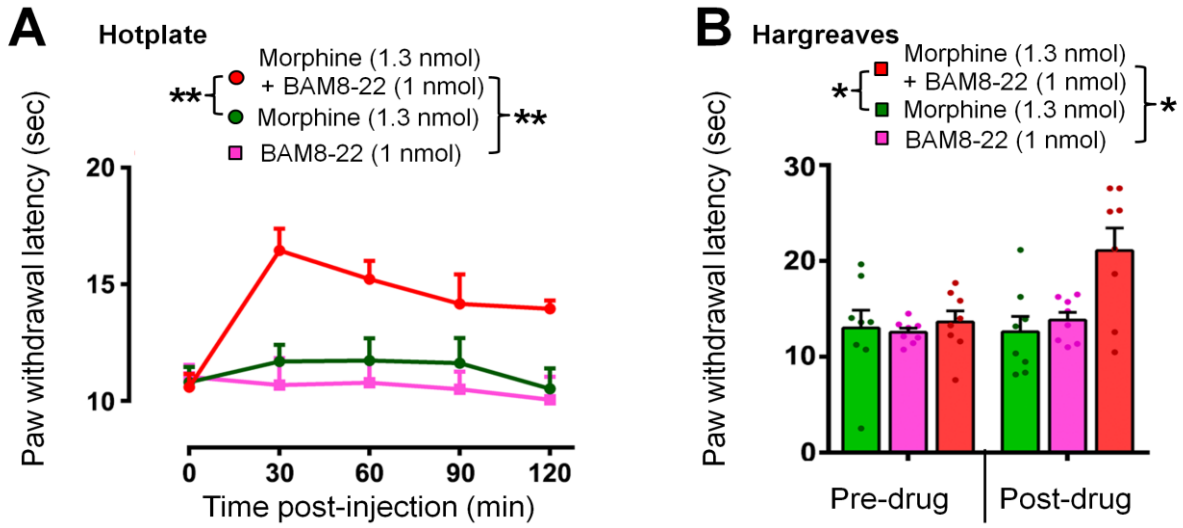

Figure S8. Intrathecal administration of BAM8-22 potentiates the inhibition of thermal nociception induced by low-dose morphine. (A) Effects of co-administration of a low dose of BAM8-22 (1 nmol, i.t.) on the pain inhibition induced by a sub-effective dose of morphine (1.3 nmol, i.t.) in the hot plate test. **(B)** Effects of co-administration of a low dose of BAM8-22 (1 nmol, i.t.) and morphine (1.3 nmol, i.t.) on heat anti-nociception in the Hargreaves test (n = 8 per group in each test). All values are mean ± SEM. *P < 0.05, **P < 0.01, two-way mixed model ANOVA and Bonferroni post hoc test.

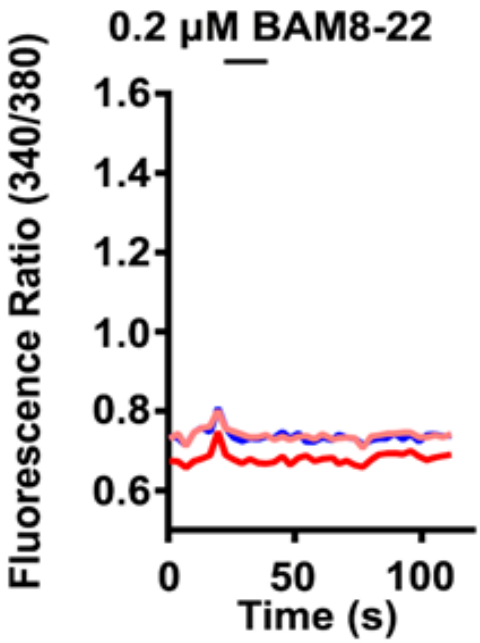

Figure S9. Low-dose BAM8-22 alone induces minimal $[Ca^{2+}]_i$ response in DRG neurons. Representative traces from cultured wild-type DRG neurons in a calcium-imaging assay show that a low dose of BAM8-22 (0.2 μM, bath application) evokes little $[Ca^{2+}]_i$ increase. Data are representative of 4 experiments.

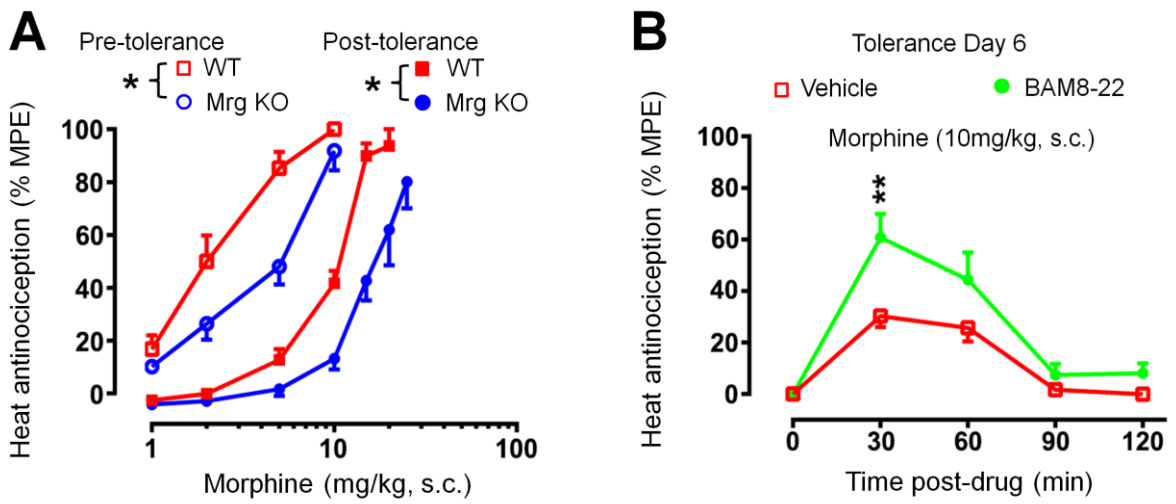

Figure S10. MrgC agonism potentiates morphine analgesia. (A) Cumulative dose-response curves for morphine-induced analgesia in wild-type (WT) and Mrg knockout (KO) mice subjected to the tail-flick test before and after chronic morphine treatment. %MPE, percent maximum possible effect. Shifts in morphine dose-effect curves after 10 days of chronic morphine treatments (10 mg/kg, s.c., daily) in WT and Mrg KO mice. Dose–response curves exhibited a 3.5-fold shift to the right of the morphine ED_{50} in the WT mice. In contrast, a more prominent 4.6-fold shift of the morphine ED_{50} was observed in Mrg KO mice (n = 7 for all groups). **(B)** The time course of the enhancement of morphine heat antinociception by intrathecal administration of BAM8-22(5 nmol, n = 7 for all groups). Repeated-measures 2-way ANOVA (A) or unpaired Student's *t* test (B) was used. All data are mean ± SEM. **P* < 0.05, ****P* < 0.001.

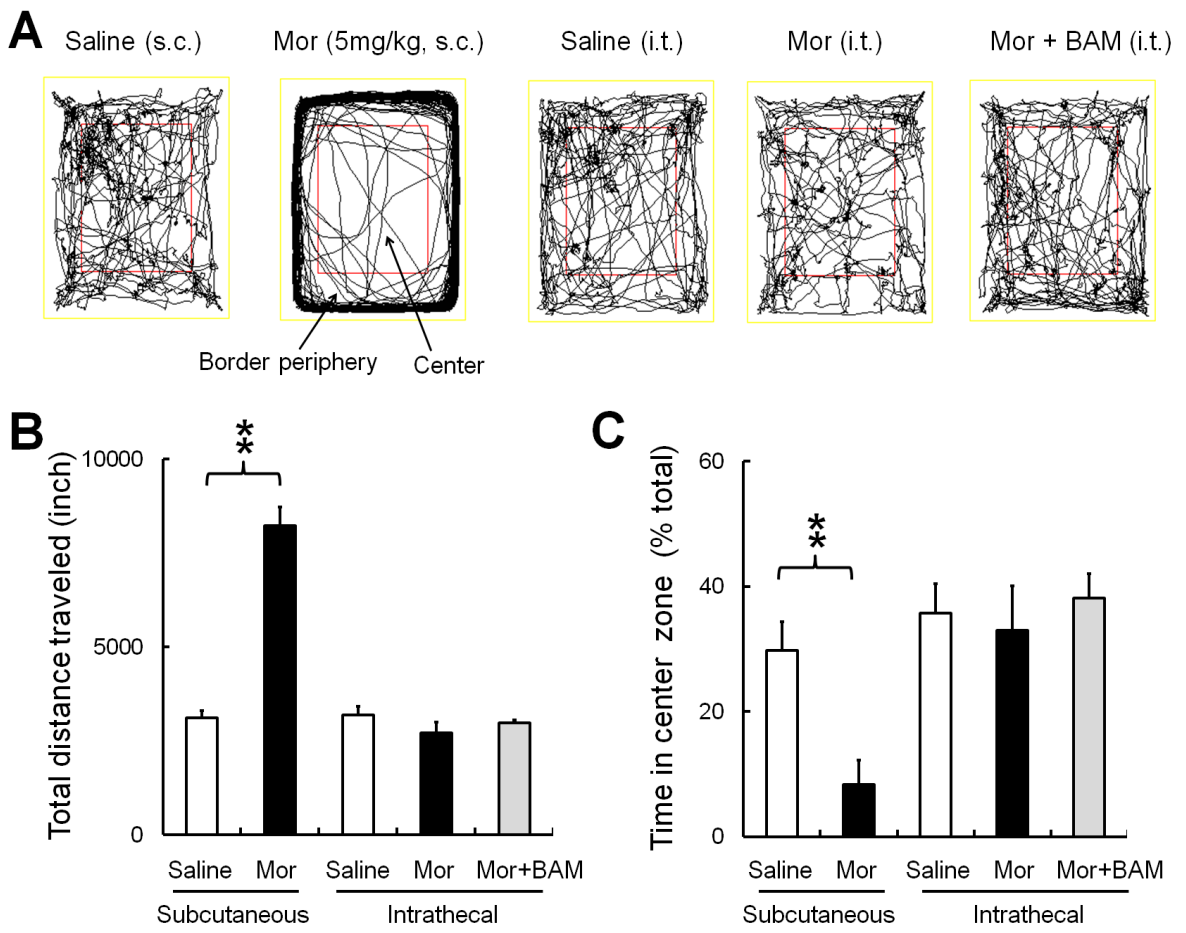

Figure S11. Intrathecal coadministration of morphine and BAM8-22 does not affect exploration activity. (A) Examples of exploration activity (10-min duration) by wild-type mice in the open field test at 45 min after drug administration. **(B)** The total distance traveled in 10 min after subcutaneous (s.c) administration of morphine (5 mg/kg) or saline control (n = 6/group). Intrathecal (i.t.) administration of morphine (1.3 nmol), alone or in combination with a low dose of BAM8-22 (BAM, 1 nmol), did not affect total distance traveled, as compared to saline control (n = 6/group). **(C)** Changes in the percent of time spent in the center zone (red box) after systemic morphine (5 mg/kg, s.c.) and intrathecal morphine (1.3 nmol) administration. Data are mean ± SEM. ***P*<0.01, Student's *t*-test.

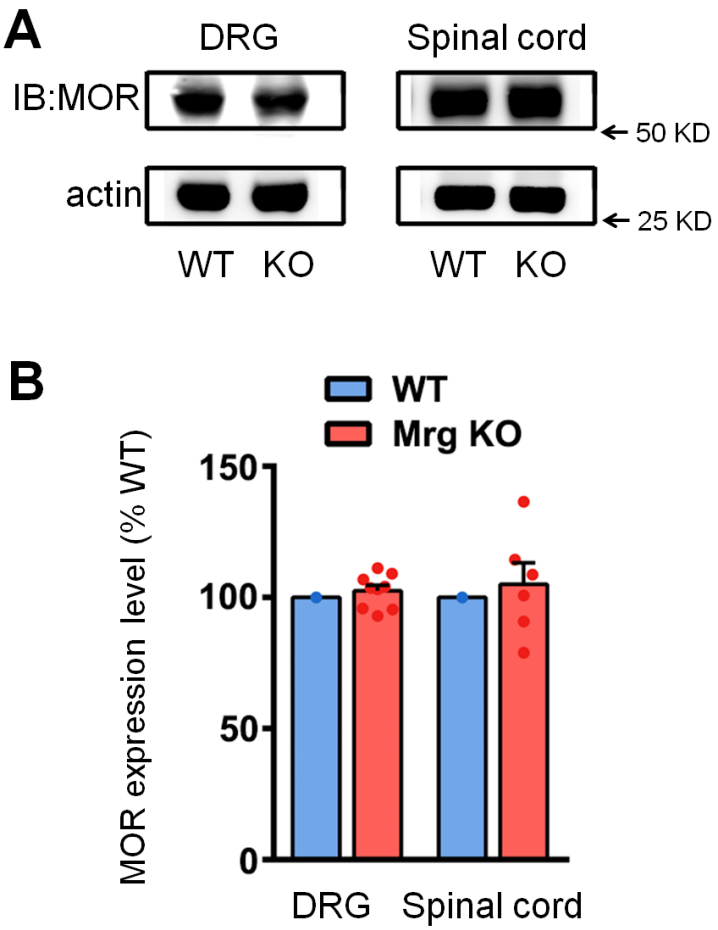

Figure S12. Expression of MOR in the DRG and spinal cord of wild-type and *Mrg* KO mice. (A) Immunoblots (IB) and **(B)** quantitative data analysis of MOR expression level between wild-type (WT) and *Mrg* knockout (KO) mice (n = 4 for both groups). Data are mean ± SEM.

Table S1. Behavior data associated with Fig. 6. CI, confidence interval; KO, knockout. n = 7 for both wild-type and Mrg KO mice.

Genotype	**Morphine ED_{50}, mg/kg (95% CI)**		
	Naive mice	Chronically treated mice	Shift (fold)
Wild-type	2.2 (1.8, 2.7)	7.6 (6.4, 9.3)	3.5
Mrg KO	3.8 (3.1, 4.7)	17.3 (12.6, 26.9)	4.6

Table S2. Primers and oligonucleotides used for plasmid construction. Primer and oligo names and sequences, 5'-3'.

	Primers
Myc-MrgC11_Forward	CCCGAATTCGGATGGATCCAACCATCTCATCCCAC
Myc-MrgC11_Reverse	TACCTCGAGATCAATATCTGCTTTCTGAAATCTC
Myc-MrgA3_Forward	CCCGAATTCGGATGGGAGAAAGCAACACCAGTGCA
Myc-MrgA3_Reverse	CCCGAATTCGGATGAACTCCACTCTTGACAGCAGC
Myc-MrgD_Forward	CCCGAATTCGGATGAACTCCACTCTTGACAGCAGC
Myc-MrgD_Reverse	TACCTCGAGATCAGACCCCATCATTAGTACACGT
FLAG-MOR_Forward	CCCGAATTCGGATGGACAGCAGCGCC
FLAG-MOR_Reverse	TACCTCGAGATTAGGGCAATGGAGCAGTTTC
MrgC11-CTD^{A3}_Forward (first round)	TTCAGGCAACGGTTGAATAAACAG
MrgC11-CTD^{A3}_Reverse (first round)	CGCGGCCGCGGTACCTCGAGATCACGGCTCTGCTTTGTTTC
MrgC11-CTD^{A3}_Forward (second round)	GGAGCCTACAAGGAAATAAATG
MrgC11-CTD^{D}_Forward (first round)	CAGAAGAGCCACCGGCTGCAGGAG
MrgC11-CTD^{D}_Reverse (first round)	CGCGGCCGCGGTACCTCGAGATCAGACCCCATCATTAGTACAC
MrgC11-CTD^{D}_Forward (second round)	GGAGCCTACAAGGAAATAAATG
MrgC11-ΔCTD_Forward	CATTGATCCCTGAAAAGA
MrgC11-ΔCTD_Reverse	CTTTCTATGCTGCCTAAA
MrgC11^{CTD}-GFP_Forward	GATCTCGAGTTTAGGCAGCATAGAAAGCATAGG
MrgC11^{CTD}-GFP_Reverse	GCAGAATTCGATATCTGCTTTCTGAAATCTCGG
MOR^{CTD}-GFP_Forward	GATCTCGAGGCGTTCCTGGATGAAAACTTC
MOR^{CTD}-GFP_Reverse	GCAGAATTCGGGGCAATGGAGCAGTTTCTG
Myc-MOR^{CTD}_Forward	CCCGAATTCGGGCGTTCCTGGATGAAAACTTC
Myc-MOR^{CTD}_Reverse	TACCTCGAGATTAGGGCAATGGAGCAGTTTC
MrgC11-TM2^{TM6}_Forward	ATCTGTGGCCTGCCTCTTGGGCTTTACTTGTTCTCTCTGCTACGGATC
MrgC11-TM2^{TM6}_Reverse	GAGGTAGACCATCACTGTGAGAGCGATGGTGATGGCTTTCCTGCG
MrgC11-TM2^{D}_Forward	TTCCTCTTCTTATTCTGCATGGCCTCCATGCTCTCTCTGCTACGGA

	TC
MrgC11-TM2^{D}_Reverse	GTCAGCCACCGCCAGGTTGAGCACATAGACGATGGCTTTCCTGCG
MOR-SmBiT_Forward	TCTGCTAGCGATGGACAGCAGCGCC
MOR-SmBiT_Reverse	CCTGAGCTCCGGGCAATGGAGCAGTTTC
LgBiT-β-arrestin-2_Forward	GTGGAGCTCAGATGGGAGAAAAACCCGGG
LgBiT-β-arrestin-2_Reverse	TCTGCTAGCCTAGCAGAACTGGTCATCACAG
MrgC11-SmBiT_Forward	TCTGCTAGCGATGGATCCAACCATCTCATCCCAC
MrgC11-SmBiT_Reverse	CCTGAGCTCCATATCTGCTTTCTGAAATCTCGGTGG
MOR^{CTD}-SmBiT_Forward	TCTGCTAGCGGCGTTCCTGGATGAAAACTTC
MOR^{CTD}-SmBiT_Reverse	CCTGAGCTCCGGGCAATGGAGCAGTTTCTG

Table S3. PCR primers. Names and sequences (5'-3') of PCR primers.

	Primers
Mrg KO_Forward1	ATGCCCAGGGAGAGCTGTAGC
Mrg KO_Forward2	AAGGTAAGCAAACATTGTTACAATG
Mrg KO_Reverse1	CCTATTGGATAATGTTCTTCCAGTG
Cre gt 3F	ATCCGTAACCTGGATAGTGAA
Pirt gt 3F	CAACTTTGTGGTACCCGAAG
Pirt gt 3R	TCCCTGGGACTCATGATGCT
MOR flox primer C	GTTACTGGAGAATCCAGGCCAAGCC
MOR flox primer C	CGCTTGGGAATATCTTGTACCTATGACCA